

# Alkanethiol Monolayers at Reduced and Oxidized Zinc Surfaces with Corrosion Protection: A Sum Frequency Generation and Electrochemistry Investigation

Hongping Zhang and Steven Baldelli\*

Department of Chemistry, University of Houston, Houston, Texas 77204

Received: August 14, 2006; In Final Form: September 26, 2006

In this work, octadecanethiol (ODT) was demonstrated to form ordered monolayers at either electrochemically reduced or oxidized Zn surfaces, by means of sum frequency generation (SFG) spectroscopy, cyclic voltammetry (CV), and electrochemical impedance spectroscopy (EIS). The SFG spectra of ODT-modified Zn electrodes featured three methyl group resonances in the C–H vibrational region (2800–3100  $\text{cm}^{-1}$ ). A significant decrease in interfacial capacitance and an increase in charge-transfer resistance were observed in EIS measurement after ODT modification. The alkane chain tilt angle of ODT within a monolayer at the Zn surface was estimated as  $0^\circ$  with respect to the surface normal by interfacial capacitance measurement via EIS. CV and SFG investigation revealed that ODT monolayers undergo reductive desorption from the Zn electrode in 0.5 M NaOH at  $-1.66$  V (vs SCE) and in 0.5 M NaClO<sub>4</sub> at  $-1.62$  V. The integrated charge consumed to the desorption of ODT is determined as 87 mC/cm<sup>2</sup> from the reductive peak on CV curve, resulting in a coverage of  $9.0 \times 10^{-10}$  mol/cm<sup>2</sup> ( $5.4 \times 10^{14}$  molecules/cm<sup>2</sup>) if assuming the reduction follows a one-electron process. ODT monolayers show corrosion protection to underlying zinc at the early immersion stage in base, salt, and acid media. However, the protection efficiency was reduced with immersion time due to the presence of defects within the monolayers.

## Introduction

Zinc is one of the most widely used metals in modern society. It has been principally used as a coating or sacrificial anode to protect steels from corrosion and rust. Zinc has also been used for die casting in the automobile industry and for roofing and gutters in building construction. Commonly, zinc coatings are further protected by the chromating process to form an inactive chromate film at the zinc surface. However, it is known that chromating formulations are carcinogenic. Enhancing the anticorrosion ability of zinc with nontoxic materials is therefore highly desired.<sup>1</sup>

On the other hand, the self-assembled monolayers (SAMs) technique is already broadly applied in nanoscience and nanotechnology, including biology, due to its strong abilities to modify surface properties and to generate novel functions. Among them, thiolate monolayers at Au, Ag, Pt, and Cu coinage metals have been intensively investigated in the past two decades.<sup>2</sup>

Recently, studies on thiol monolayers at engineering metal<sup>3–6</sup> and metal oxide<sup>7–12</sup> surfaces have attracted much interest. Delhalle's group has most recently reported X-ray photoelectron spectroscopy studies of the deposition of *n*-dodecanethiol and 3-perfluorooctyl-propanethiol at electrochemically reduced Zn surfaces.<sup>1</sup>

This work presents the formation of octadecanethiol (ODT) monolayers at reduced Zn and oxidized Zn surfaces. The ODT monolayers at both zinc surfaces were characterized by sum frequency generation (SFG) spectroscopy. The alkane chain cant angle of ODT at the Zn surface was estimated by electrochemical impedance spectroscopy (EIS) measurements. Cyclic vol-

tammety (CV) and SFG were employed to study reductive desorption of ODT from the Zn electrode. The anticorrosion effects of these systems were evaluated by means of EIS in acid, salt, and base solutions, respectively.

## Experimental Section

**Materials.** Commercially available ODT (98%, Aldrich) and ethanol (absolute-200 proof, Aaper) were used as received. A zinc rod (99.9999%, 9.45 mm in diameter, 0.70 cm<sup>2</sup> in geometric surface area) was purchased from Alfa Aesar and mounted in a Teflon sheath, exposing only the circular cross-section.

**Electrode and Monolayer Preparation.** Zn electrodes were first polished by 1000 grit emery paper and further polished with a 6, 3, and 1 mm diamond suspension sequentially. Zn electrodes used in the EIS measurement for evaluating the anticorrosion effect were only polished with 1000 grit emery paper. Before using, the freshly polished electrode was rinsed, ultrasonicated with acetone for 5 min, and then rinsed with water from a Millipore A10 system ( $>18$  M $\Omega$  cm<sup>2</sup>).

Figure 1 shows CV curves of the Zn electrodes in different solutions that determined the reduction and oxidation potentials in this work to form reduced Zn and oxidized Zn surfaces. While Zn begins to passivate after potential positive to  $-1.1$  V in NaOH solution, there is no passivative film forming in acid solution.

In the case of the reduced Zn electrode (labeled as Zn<sub>re</sub>), the clean Zn electrode was introduced into a three-electrode glass cell containing electrolyte purged with a pure N<sub>2</sub> gas flow. A Pt wire coil and saturated calomel electrode (SCE) were used as the counter electrode and reference electrode, respectively. The electrolytes used to reduce Zn electrodes include 1 M NaOH, 1 M Na<sub>2</sub>CO<sub>3</sub>, 0.5 M NaClO<sub>4</sub>, or 0.5 M HClO<sub>4</sub> aqueous solutions. A cathodic potential, which was chosen on the basis of the CV curves in an associated solution shown in Figure 1,

\* To whom correspondence should be addressed. E-mail: sbaldelli@uh.edu.

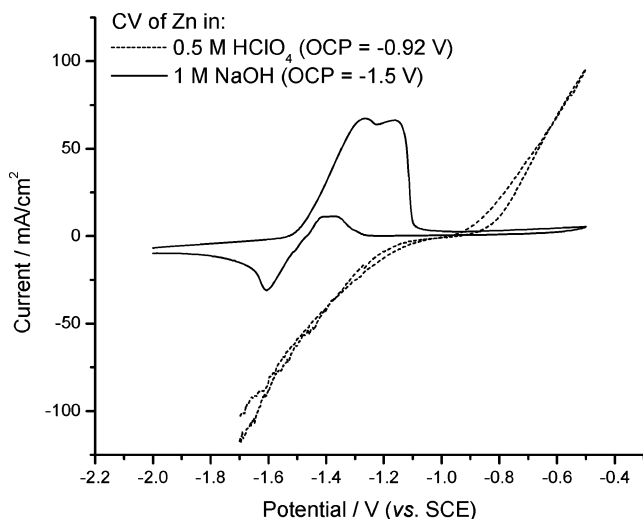


**Figure 1.** Cyclic voltammograms of a Zn electrode in various electrolytes with a scan rate of 100 mV/s.

was applied on the Zn electrode for 30 min to reduce the native oxide layer at the Zn surface. For example, the applied reduction potential was  $-1.3$  V in  $\text{HClO}_4$  and  $-1.7$  V in  $\text{NaOH}$  solutions, respectively. The reduced Zn electrode was taken out of the solution under  $\text{N}_2$  gas protection and quickly rinsed with ethanol and immersed into 1 mM ODT deaerated ethanol solution as quickly as possible. The immersion time was typically more than 1 h. We note that similar SFG spectra were observed for the samples with longer immersion times, up to 8 h. After ODT deposition, the electrode was rinsed, ultrasonicated, rinsed with ethanol, and dried with  $\text{N}_2$  gas flow. SFG and electrochemical measurements were performed within 5 min after ODT monolayers were prepared.

The oxidized Zn electrodes (labeled as  $\text{Zn}_{\text{ox}}$ ) for the formation of ODT monolayers were prepared by electrochemical (EC) and thermal (TH) methods.  $\text{Zn}_{\text{ox}}$  film was obtained by anodizing a Zn electrode in 1 M  $\text{NaOH}$  solution at  $-1.0$  V where Zn was passivated according to the CV curve shown in Figure 1. The typical oxidation charge was  $300 \text{ mC/cm}^2$ . A thin white transparent oxide layer was then obtained at the Zn electrode surface. This passive film was comprised of  $\text{ZnO}$  and/or  $\text{Zn}(\text{OH})_2$ .<sup>13–16</sup> Assuming that the passivating film consisted of  $\text{ZnO}$  and taking the density ( $\rho$ ) of this porous film as  $4.0 \text{ g/cm}^3$ ,<sup>17</sup> the thickness ( $d$ ) of the passivating film can be estimated by Faraday's law:

$$d = \frac{MQ}{nF\rho A} \quad (1)$$

where  $M$  is the molar mass of  $\text{ZnO}$  ( $81.4 \text{ g/mol}$ ),  $Q$  is the charge consumed on formation of the passivating layer,  $n$  is the number of electrons involved in film formation (here,  $n = 2$ ),  $F$  is Faraday's constant ( $96500 \text{ C/mol}$ ), and  $A$  is the surface area of the Zn electrode ( $0.7 \text{ cm}^2$ ). Hence, the average thickness of the passivating layer at Zn surface was approximately  $450 \text{ nm}$ . The thermally oxidized Zn film was formed by heating a clean Zn electrode to  $110 \text{ }^\circ\text{C}$  in air for  $0.5$ – $1$  h. Prior to the start of ODT deposition, the fresh  $\text{Zn}_{\text{ox}}$  film electrode was rinsed with ethanol and dried with  $\text{N}_2$  gas flow. The  $\text{Zn}_{\text{ox}}$  film electrode was immersed in a 1 mM ODT/EtOH solution overnight in order to obtain high quality SFG spectra.

**SFG Experiment.** SFG spectra were collected in air on a homemade setup with copropagating optical configuration as described previously,<sup>5</sup> in which the incidence angles of the visible and IR beams are  $45$  and  $60^\circ$ , respectively. The scan

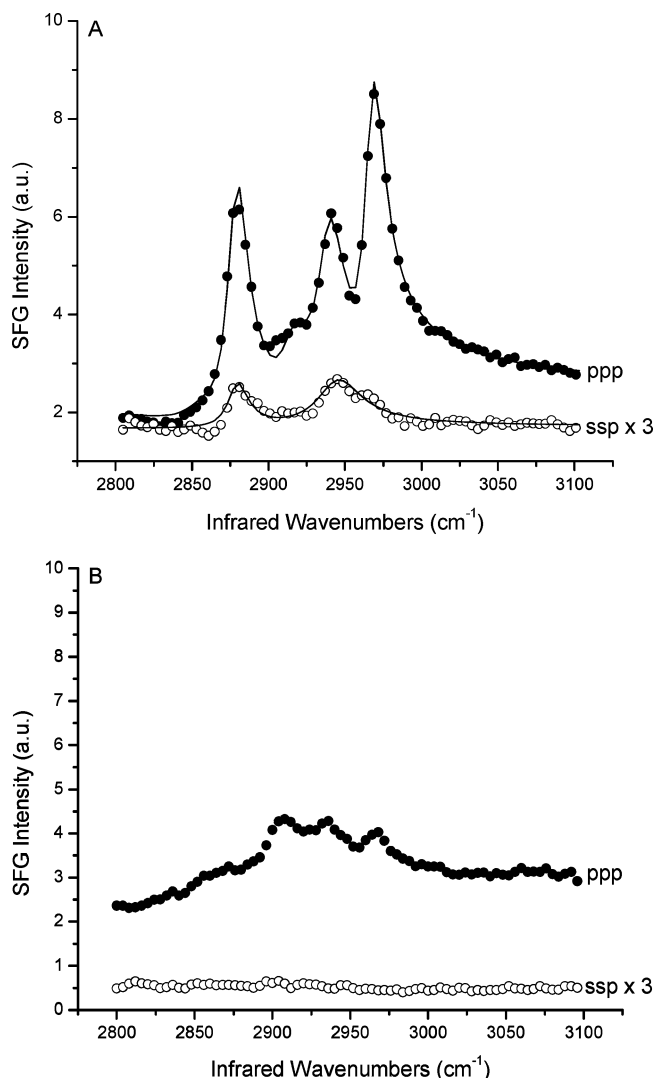


**Figure 2.** SFG spectra of Zn electrodes: (A) ODT modified  $\text{Zn}_{\text{ne}}$ , the solid line is curve of fit to eq 2; (B) ODT-uncoated  $\text{Zn}_{\text{ne}}$  after immersion in pure ethanol for 1 h.

rate was  $1 \text{ cm}^{-1}/\text{s}$ , and the repetition rate was  $20 \text{ Hz}$ . The visible beam was produced via the  $1064 \text{ nm}$  beam being frequency doubled to  $532 \text{ nm}$ . Two polarization combinations (ppp and ssp) spectra were acquired in the C–H stretching region from  $2800$  to  $3100 \text{ cm}^{-1}$ . Each presented spectrum was an average of five scans. The SFG spectra were curve fit by Origin 6.0 using the following equation

$$I_{\text{SFG}} \propto |\chi_{\text{NR}}^{(2)} + \chi_{\text{R}}^{(2)}|^2 = \left| \chi_{\text{NR}}^{(2)} + \sum_q \frac{A_q}{\omega_{\text{IR}} - \omega_q + i\Gamma_q} \right|^2 \quad (2)$$

where  $\chi_{\text{NR}}^{(2)}$  and  $\chi_{\text{R}}^{(2)}$  are the nonresonant susceptibility attributed to the metal substrate and the resonant susceptibility due to adsorbed monolayer, respectively.  $A_q$ ,  $\omega_{\text{IR}}$ ,  $\omega_q$ , and  $\Gamma_q$  are the amplitude, the scanning IR frequency, the  $q$ -th resonant vibrational frequency of the adsorbates, and the line width, respectively.

**Electrochemistry.** An EG&G PAR M263A potentiostat was used to reduce and to oxidize the Zn electrodes. CV and EIS measurements were performed with the M263A potentiostat in combination with a PAR M5210 lock-in amplifier controlled by PowerSuite software. EIS measurement was performed at open circuit potential (OCP) with an amplitude of the applied sinusoidal signal of  $10 \text{ mV}$ . The scan range of frequency was

**TABLE 1: Fitting Results of the SFG Spectra Obtained in Air from ODT-Modified Zinc Electrodes**

electrode	spectrum	ODT/Zn <sub>re</sub>	ODT/Zn <sub>re</sub>	ODT/Zn <sub>ox</sub>	ODT/Zn <sub>ox</sub>	ODT/Zn <sub>ox</sub>	ODT/Zn <sub>ox</sub>
		Figure 2A ppp	Figure 2A ssp	fresh polished Zn Figure 3 spectrum a	anodized Zn with $Q_{ox} = 30$ mC/cm <sup>2</sup> Figure 3 spectrum b	anodized Zn with $Q_{ox} = 300$ mC/cm <sup>2</sup> Figure 3 spectrum c	thermal Zn Figure 3 spectrum d
CH <sub>3,s</sub>	A	9.7	1.5	4.9	6.1	6.0	5.5
	Γ	8.3	8.0	8.3	8.8	8.8	8.8
	(A/Γ) <sup>2</sup>	1.4	0.035	0.35	0.48	0.46	0.39
CH <sub>3,Fermi</sub>	A	9.2	3.5	6.1	8.8	7.5	6.9
	Γ	11	18	11	13	13	13
	(A/Γ) <sup>2</sup>	0.70	0.038	0.31	0.46	0.33	0.28
CH <sub>3,as</sub>	A	9.0		5.2	6.3	6.8	6.2
	Γ	7.7		7.7	8.0	8.0	8.0
	(A/Γ) <sup>2</sup>	1.4		0.46	0.62	0.72	0.60
CH <sub>2,s</sub>	A	1.5		0	1.7	1.8	0.42
	Γ	15		15	13	20	5.0
	(A/Γ) <sup>2</sup>	0.01		0	0.02	0.008	0.007
CH <sub>2,as</sub>	A	3.8		2.3	3.0	3.8	3.6
	Γ	11		15	10	15	15
	(A/Γ) <sup>2</sup>	0.12		0.02	0.09	0.064	0.058
	χ <sub>NR</sub>	1.6	0.75	1.2	1.3	1.4	2.0
	<i>j</i> <sub>NR</sub>	−50°	−76°	−34°	0°	11°	21°

**TABLE 2: Averaged Fitting, Simulation, and Calculation Results of the EIS Data Obtained at an ODT Modified Zn (Reduced) and Au Electrodes in Deaerated 0.5 M NaClO<sub>4</sub> Solution**

electrode	$Q_{dl}$		$f_{max}$ (Hz)	calculated $C_{dl}$ (mF cm <sup>−2</sup> )	$R_{ct}$ (W cm <sup>2</sup> )
	$Q_0$ (W <sup>−1</sup> cm <sup>−2</sup> s <sup><i>n</i></sup> )	<i>n</i>			
ODT/Zn <sub>re</sub>	$2.06 \times 10^{-6}$	0.93	7.28	1.58	15 k
ODT/Au	$1.87 \times 10^{-6}$	0.95	0.16	1.87	480 k

from 100 kHz to 10 or 0.1 Hz. The inhibition efficiencies of the ODT monolayers were evaluated in aerated 0.1 M HCl, 0.5 M NaCl, and 1 M NaOH aqueous solutions, respectively. The impedance data were fit to a suitable equivalent circuit (EC) by ZSimpWin software. All potentials were reported vs the SCE. All experiments were performed at room temperature.

## Results and Discussion

**SFG of ODT/Zn<sub>re</sub>.** Figure 2A shows the ppp and ssp SFG spectra obtained from an ODT-modified Zn<sub>re</sub> electrode in air. The SFG spectra of the bare Zn<sub>re</sub> electrode are also shown for the purpose of comparison (Figure 2B) and clearly demonstrate that neither solvent (ethanol) nor hydrocarbon contamination in air introduced a comparable contribution to the observed SFG of the ODT/Zn<sub>re</sub> electrode. In the previous observation of the SFG spectra of the ODT/Au system in our lab, three resonances appeared as “dips” in the ppp spectrum at 2879, 2938, and 2967 cm<sup>−1</sup> and two resonances appeared as dips in the ssp spectrum with the absence of the antisymmetric mode.<sup>5</sup> However, the ppp spectrum of the ODT-modified Zn<sub>re</sub> electrode shown in Figure 2A exhibits three strong resonant peaks in the region of C–H stretching at 2878, 2938, and 2967 cm<sup>−1</sup> that are in the opposite direction to the case of the ODT/Au system. These three peaks can be respectively attributed to the symmetric, Fermi resonance, and antisymmetric modes of the terminational methyl group of ODT.<sup>18</sup> The ssp spectrum in Figure 2A shows two profound peaks at 2881 and 2945 cm<sup>−1</sup> that are assigned to the symmetric vibration and Fermi resonance of the methyl groups pointing away from the surface. Therefore, SFG results demonstrated the adsorption of the ODT at the electrochemically reduced Zn surface and the formation of the ordered monolayers. This was further verified by the decrease in the interfacial capacitance and the increase in the charge-transfer resistance as discussed later (see Tables 2 and 3). However, there are two weak peaks in the ppp spectrum appearing at 2850 and 2916 cm<sup>−1</sup> that

belong to the methylene groups. Their appearance is usually considered as the indicator gauche defects on the chains in the monolayers,<sup>18–20</sup> possibly originating from collapsed sites and pinhole defects within the ODT monolayer structure.<sup>21</sup> ODT molecules may not densely pack and order at collapsed sites and around pinholes leading to the observation of methylene group’s vibration modes in the SFG spectra.

From the fitting parameters of the SFG spectra, the nonresonant phases (*j*<sub>NR</sub>) of reduced Zn substrates are determined, respectively, as −50 and −76° for ppp and ssp spectra; these values are different from that of ODT/Au in our previous work (the values of *j*<sub>NR</sub> for Au are 90 and 60° for ppp and ssp spectra, respectively). As it is known, the nonresonant phase of the metal is one of the factors that determines the resonant line shape in a SFG spectrum.<sup>5,18</sup>

It is noteworthy that the electrolytes used to reduce Zn surfaces have no obvious effect on the SFG spectra obtained from the ODT/Zn<sub>re</sub> electrodes where Zn electrodes were reduced in HClO<sub>4</sub>, NaClO<sub>4</sub>, Na<sub>2</sub>CO<sub>3</sub>, and NaOH solutions, respectively.

**SFG of ODT/Zn<sub>ox</sub>.** In the present work, electrochemical and thermal methods were used to prepare Zn<sub>ox</sub> thin film substrates for ODT deposition. In Figure 3, spectrum a was obtained from a freshly polished Zn electrode that was modified with ODT. Curves b and c are SFG spectra of the ODT/Zn<sub>ox</sub> electrodes where Zn<sub>ox</sub> films were formed at −1.0 V with different oxidation charges (30 and 300 mC/cm<sup>2</sup>, respectively). As for spectrum d, the Zn<sub>ox</sub> film was obtained by heating a clean Zn electrode at 110 °C in air for 1 h. Similar to the case of ODT/Zn<sub>re</sub>, all of these spectra show three strong −CH<sub>3</sub> group resonances and two −CH<sub>2</sub> group resonances in the C–H vibrational region. However, these spectra display various nonresonant phases (*j*<sub>NR</sub>) and amplitudes that clearly distinguish them from the ODT/Zn<sub>re</sub> electrode. The fitting results estimated that the values of *j*<sub>NR</sub> are −34, 0, 11, and 21° for spectra a, b, c, and d, respectively. The observation of strong methyl group resonances in SFG spectrum indicated that ODT can bond to Zn<sub>ox</sub> thin film surfaces and form ordered monolayers with polar orientation, which is detected by SFG spectroscopy. EIS experiments provide further evidence to support this conclusion. As shown in Table 2, after the modification of ODT, the double layer capacitances ( $C_{dl}$ ) of the Zn<sub>ox</sub> film electrodes dramatically decreased to 1.24 from 27.9 mF/cm<sup>2</sup> in 0.1 M HCl solution and to 0.75 from 15.0 mF/cm<sup>2</sup> in 0.5 M NaCl solution. Moreover, the charge-transfer resistances ( $R_{ct}$ ) increased more than 15 times as compared to the ODT-uncoated Zn<sub>ox</sub> film

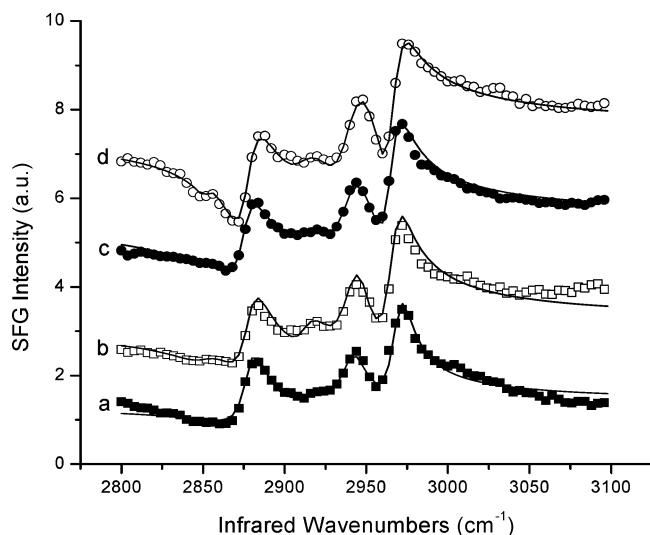


**Figure 3.** ppp-SFG spectra of ODT modified  $Zn_{ox}$  thin film electrodes that formed under various conditions. (a) Freshly polished Zn electrode without reduction. (b) Anodized at  $-1.0$  V in  $1$  M NaOH with oxidation charge of  $30$   $mC/cm^2$ . (c) Anodized at  $-1.0$  V in  $1$  M NaOH with oxidation charge of  $300$   $mC/cm^2$ . (d) Zn electrode was heated at  $110$  °C in air for  $1$  h. All  $Zn_{ox}$  electrodes were immersed in  $1$  mM ODT/EtOH solution for  $24$  h before the SFG measurement. Spectra b, c, and d have been offset vertically by  $+1.5$ ,  $+3.5$ , and  $+3.5$  for clarity. The solid lines are curves of fit from eq 2.

electrode in  $0.1$  M HCl and  $0.5$  M NaCl solutions. It is known that the significant changes in  $C_{dl}$  and  $R_{ct}$  are characteristic of the formation of long chain organic monolayers at electrodes.<sup>5,21–23</sup>

However, it was found that a longer immersion time was required to form a well-defined ODT monolayer at  $Zn_{ox}$  films in order to generate a high quality SFG spectrum, which is probably due to longer times being preferable to ODT to reduce Zn oxide to form an ordered thiolate monolayer at the  $Zn_{ox}$  thin film surface.

**Chain Tilt Angle of ODT Molecules in Monolayer at the Zinc Surface.** Chain tilt angle or cant angle ( $\alpha$ ), namely, the angle between the axis of the hydrocarbon backbone and the surface normal, is one of the important parameters describing the orientation of the organic molecules in SAMs. Thiolate SAMs display different cant angles at different substrates. For example, it has been found that the cant angle of alkanethiol at Au is  $\sim 30^\circ$ , while this value for Ag, Cu, and Pt is between  $10$  and  $15^\circ$ .<sup>2</sup> It has also been reported that alkanethiols orient perpendicularly at the mercury surface ( $\alpha \gg 0^\circ$ ).<sup>24</sup> In this work, the cant angle of ODT at the Zn surface was estimated by interfacial capacitance obtained from EIS measurements. Figure 4 shows Nyquist plots of an ODT/ $Zn_{re}$  electrode and an ODT/Au electrode in a deaerated  $0.5$  M NaClO<sub>4</sub> solution, respectively. The associated ECs used to fit the EIS data are shown in the inset. In this work, Mensfield's equation<sup>25</sup>

$$C = Q_0(2\pi f_{max})^{n-1} \quad (3)$$

was employed to convert the value of the constant phase element to a capacitor as in our previous work.<sup>5</sup> Here,  $f_{max}$  is the frequency at which the imaginary part of the Nyquist plot reaches a maximum. The fitting and calculation results are listed in Table 2.

The average capacitance values of the ODT monolayer at the reduced Zn electrode are  $1.58$  ( $\pm 5.3\%$ ) and  $1.87$   $mF/cm^2$

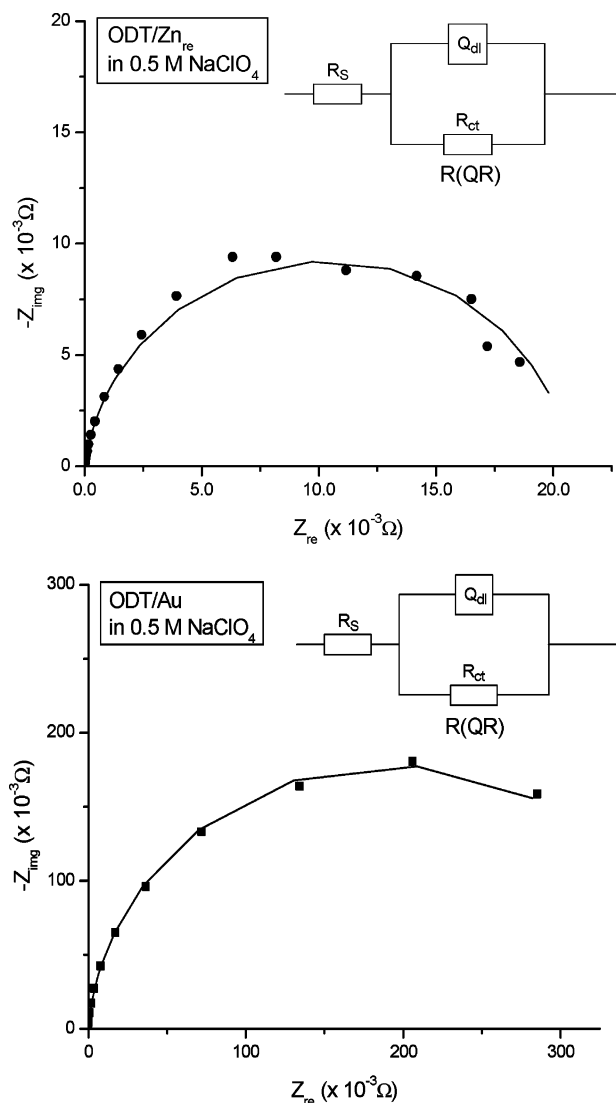


**Figure 4.** Nyquist plots of the ODT/ $Zn_{re}$  electrode (top,  $100$  k to  $1$  Hz) and an ODT/Au electrode (bottom,  $100$  k to  $0.1$  Hz) in deaerated  $0.5$  M NaClO<sub>4</sub> solutions. The surface areas of the Zn and Au electrodes are  $0.70$  and  $1.25$   $cm^2$ , respectively.

( $\pm 2.4\%$ ) at the Au electrode. Therefore, the cant angle of ODT at the Zn surface can be estimated by the following equation:

$$\cos\alpha_{ODT/Zn} = \frac{C_{SAM,ODT/Au}}{C_{SAM,ODT/Zn}} \cos\alpha_{ODT/Au} \quad (4)$$

Taking  $\alpha_{ODT/Au} = 30^\circ$ , then  $\cos\alpha_{ODT/Zn} = 1.02$ . Within the errors of experiment and of the theoretical treatment, it can be taken that  $\cos\alpha_{ODT/Zn} \gg 1$ , thereby  $\alpha_{ODT/Zn} = 0^\circ$ .

**Reductive Desorption of ODT Monolayer from Zinc Surface.** Thioliates at gold surfaces have been reported to undergo reductive desorption through a one-electron process at very negative potentials in neutral or basic solution.<sup>26–35</sup> For example, it has been reported that the reductive desorption peak of thiolate monolayers at Au electrode is at ca.  $-1.1$  V in base solution.<sup>28,30,32</sup>

The reductive desorption behavior of ODT monolayers at the reduced Zn electrode was investigated in this work by means of CV and SFG. As shown in Figure 5A (dotted line), the bare  $Zn_{re}$  electrode gave only one reduction peak at ca.  $-1.44$  V in  $0.5$  M NaOH solution when the electrode potential is scanned negatively from  $-1.4$  to  $-1.8$  V. This peak corresponds to the

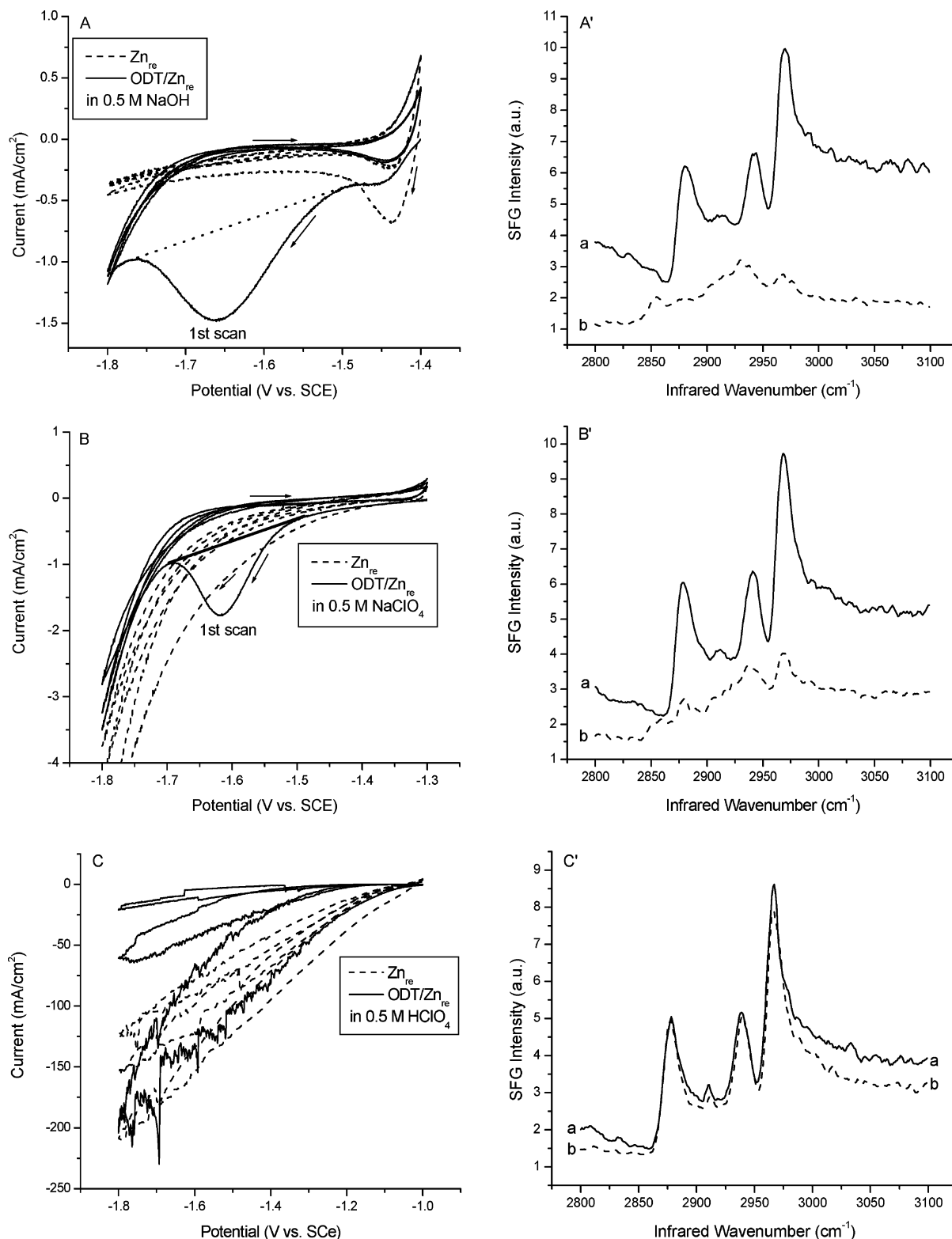


**Figure 5.** Cyclic voltammograms (left column) of the ODT modified reduced Zn electrodes (solid lines) and the reduced Zn electrodes (dotted lines) in deaerated 0.5 M NaOH (A), 0.5 M NaClO<sub>4</sub> (B), and 0.5 M HClO<sub>4</sub> (C) solutions with a scan rate of 100 mV/s. The arrows indicate the direction of the potential sweeping. The dashed lines show the baselines for current integration. The right column gives the ppp SFG spectra of the ODT-modified reduced Zn electrodes before (spectra a) and after (spectra b) potential cycle sweeping in the corresponding solutions.

reduction of the electrochemically oxidized zinc species. The current of the peak increased with the positive starting potential (not shown). On the contrary, upon the first negative scan (Figure 5A, solid line) of an ODT/Zn<sub>re</sub> electrode in 0.5 M NaOH solution, a new irreversible peak appeared on the CV curve at ca. -1.66 V that disappeared on the second scan. This reduction

peak, starting from -1.49 V and ending at -1.76 V, was attributed in the present work to the reductive desorption of the ODT monolayer from the Zn electrode. This conclusion was supported by SFG measurements in the present work. The ODT/Zn<sub>re</sub> electrode, after undergoing three CV scans between -1.4 and -1.8 V in 0.5 M NaOH, gave a SFG spectrum (Figure

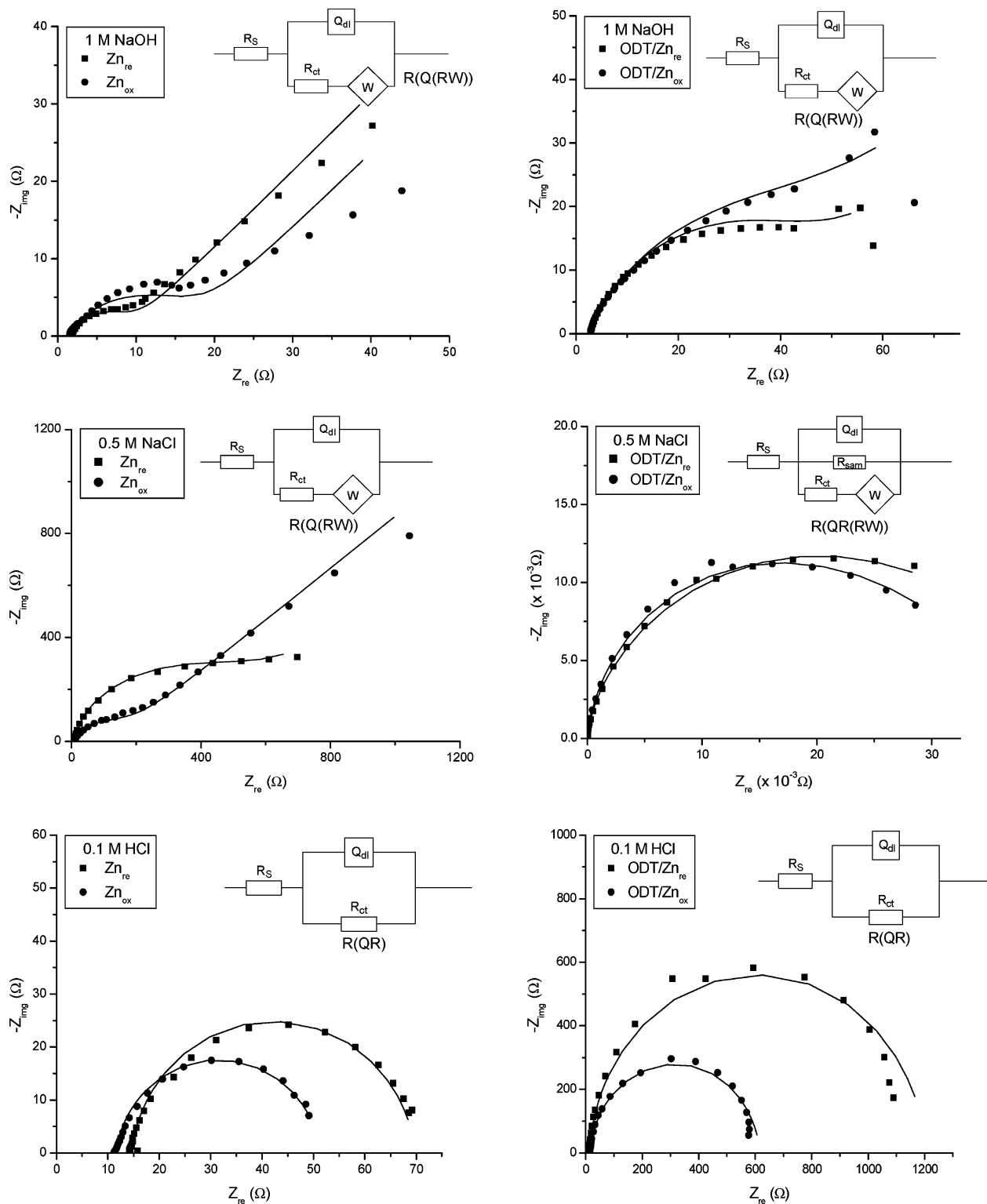


**Figure 6.** Nyquist plots of Zn (left column) and ODT-coated Zn (right column) electrodes recorded at OCP within 10 min after immersion in 1 M NaOH, 0.5 M NaCl, and 0.1 M HCl solutions. The solid lines are fit curves.

5A', spectrum b) with poorly detectable signals as compared to those from a fresh ODT/Zn<sub>re</sub> electrode (Figure 5A', spectrum a), verifying the desorption of ODT monolayers from the Zn surface. In a 0.5 M NaClO<sub>4</sub> solution, a similar behavior was also observed in the CV curve and in the SFG spectra for the ODT/Zn<sub>re</sub> electrodes (Figures 5B and 6B'), indicating that reductive desorption of ODT monolayer from the Zn electrode is able to take place in neutral solution. In Figure 5B, the reduction peak centered at ca. -1.62 V, starting from -1.48 V

and ending at -1.69 V. The total charges ( $Q_t$ ) under the reduction peaks were determined by integration of the peak area. The dashed lines in Figures 5A and 6B show the baselines for integration. The values of  $Q_t$  are 95.6 mC/cm<sup>2</sup> in 0.5 M NaOH and 93.4 mC/cm<sup>2</sup> in 0.5 M NaClO<sub>4</sub>, respectively. These values are consistent with the results in the case of thiol-modified Au electrodes reported in the literature.<sup>26,27,29,31-33</sup> Considering that the double-layer charging ( $Q_{dl}$ ) also contributed to the total charge, it is necessary to subtract the value of  $Q_{dl}$  from  $Q_t$  to

obtain the Faradaic charge. In this work, the value of  $Q_{dl}$  was estimated by the method described in the literature<sup>30,32</sup> as follows:

$$Q_{dl} = Q_{dl,M} - Q_{dl,SAM/M} \\ = (E_{str} - PZC_M)C_M - (E_{ini} - PZC_{SAM/M})C_{SAM/M} \quad (5)$$

where  $Q_{dl,M}$  and  $Q_{dl,SAM/M}$  are the double-layer charges consumed by uncoated and thiol-coated metal electrodes;  $PZC_M$  and  $PZC_{SAM/M}$ ,  $C_M$ , and  $C_{SAM/M}$  are the potentials of zero charge and double-layer capacitances for the bare metal and the thiol-covered metal electrodes, respectively;  $E_{str}$  is the potential just after the thiol stripping peak; and  $E_{ini}$  is the initial potential of the CV. For example, in the case of 0.5 M NaClO<sub>4</sub> solution,  $E_{str}$  is  $-1.69$  V as determined from CV (Figure 5B),  $PZC_{Zn}$  is  $-1.16$  V ( $-0.92$  V vs NHE) from literature,<sup>36</sup> and the average  $C_{Zn}$  is  $12.0$  mF/cm<sup>2</sup> obtained from our EIS measurements. As an approximation, the contribution of  $Q_{dl,SAM/M}$  was ignored in this work due to the fact that the values of the  $C_{ODT/Zn}$  ( $1.58$  mF/cm<sup>2</sup> in 0.5 M NaClO<sub>4</sub>; see Table 2) are almost 1 order of magnitude smaller than those of the bare Zn<sub>re</sub> electrode ( $12.0$  mF/cm<sup>2</sup>). Therefore,  $Q_{dl} \gg Q_{dl,M} = 6.4$  mC/cm<sup>2</sup>. Finally, the charge consumed in stripping ODT from the Zn electrode is approximately  $87$  mC/cm<sup>2</sup>, which results in a coverage of  $9.0 \times 10^{-10}$  mol/cm<sup>2</sup> ( $5.4 \times 10^{14}$  cm<sup>-2</sup> in molecular density) assuming that the reduction follows one-electron process. However, there is no visible reductive desorption peak appearing on the first negative scan in 0.5 M HClO<sub>4</sub> solution for the ODT/Zn<sub>re</sub> electrode (Figure 5C). After undergoing six potential cyclic scans between  $-1.0$  and  $-1.8$  V at  $100$  mV/s, the SFG spectrum of the ODT-modified Zn electrode (Figure 5C') did not show an obvious difference from the same ODT/Zn<sub>re</sub> electrode before the CV treatment. These results probably indicate no reductive desorption taking place in acidic solution even in the vigorous hydrogen evolution region (see the noised CV curve), which is consistent with the observation of thiol SAMs at Au electrodes that thiol monolayer reductive desorption does not take place in acid.<sup>35</sup>

**Anticorrosion Effect of the ODT Monolayers at Zinc Surfaces.** It has been reported that alkanethiol SAMs at copper,<sup>37–39</sup> iron,<sup>40</sup> mild steel,<sup>5</sup> and gold<sup>41</sup> can protect underlying metals against corrosion. The anticorrosion effects of the ODT monolayers on the underlying zinc in different media were evaluated in this work by means of EIS.

Figure 6 presents a set of complex-plane plots of the impedance of bare zinc (Zn<sub>re</sub> and Zn<sub>ox</sub>, left column) and ODT-modified zinc (ODT/Zn<sub>re</sub> and ODT/Zn<sub>ox</sub>, right column) electrodes obtained at corrosion potential in 0.1 M HCl, 0.5 M NaCl, and 1 M NaOH solutions, respectively. EIS data were acquired within 10 min after the immersion of the electrodes in the solutions. The impedance data were fitted to an appropriate EC such as  $R(QR)$ ,  $R[Q(RW)]$ , or  $R[QR(RW)]$  (see the insets in Figure 6), where  $R_s$  is the solution resistance between the working and the reference electrodes.  $R_{ct}$  represents the charge-transfer resistance whose amplitude reflects the ability of the Zn electrode against corrosion reaction.  $Q_{dl}$  is the constant phase element used to modify the double-layer capacitance ( $C_{dl}$ ) of the zinc electrode in the EC for the purpose of obtaining more accurate fitting results.  $W$  is the Warburg impedance induced by the diffusion of corrosive reactants or corrosion product species.  $R_{SAM}$  reflects the resistance of the ODT monolayers to the transformation of the electrons.

All of the Nyquist plots of bare zinc and ODT monolayer-modified zinc electrodes measured in 0.1 M HCl display simple

**TABLE 3: Fitting and Calculation Results of the EIS Obtained at Zn and ODT-Modified Zn Electrodes in 0.1 M HCl, 0.5 M NaCl, and 1 M NaOH Solutions**

solution/ electrode	$\chi^2$ (%)	$Q_{dl}$ (W <sup>-1</sup> cm <sup>-2</sup> s <sup>n</sup> )	$n$	$f_{max}^a$ (Hz)	$C_{dl}^b$ (mF cm <sup>-2</sup> )	$R_{ct}$ (W cm <sup>2</sup> )	IE <sup>c</sup> (%)
1 M NaOH							
Zn	4.3	829	0.76	193	151	5.44	/
ODT/Zn	8.5	256	0.72	106	41.4	34.2	84.1
ZnO	18	1653	0.66	54.4	227	11.6	/
ODT/ZnO	14	376	0.69	208	40.6	39.3	70.5
0.5 M NaCl							
Zn	3.9	70.1	0.93	8.5	53.0	371	/
ODT/Zn	6.8	0.83	0.96	7.3	0.71	4028	90.8
ZnO	4.4	29.4	0.84	99	15.0	109	/
ODT/ZnO	9.1	0.95	0.94	7.3	0.75	10580	99.0
0.1 M HCl							
Zn	4.1	35.7	0.93	174.3	21.9	38.7	/
ODT/Zn	7.5	1.03	0.96	239.5	0.77	833	95.4
ZnO	2.1	65.56	0.92	174.3	23.9	27.9	/
ODT/ZnO	5.9	1.81	0.95	329.0	1.24	420	93.4

<sup>a</sup> Note: If  $Q$  was used for fitting, then  $C$  was estimated by Mansfeld's equation. <sup>b</sup>  $f_{max}$  was deduced from simulation of the (QR) part included in the EC. <sup>c</sup> IE (Inhibition efficiency) was calculated with the equation: IE (%) =  $R_{ct,ODT} - R_{ct,blk}/R_{ct,ODT} \times 100$  (6).

capacitive loops with only one time constant in Bode diagrams (not shown), indicating a fast and simple dissolution process. The impedance data in 0.1 M HCl were well-fit to  $R(QR)$ . The impedance data of bare zinc electrodes in 0.5 M NaCl were fitted to  $R[Q(RW)]$  due to the appearance of the straight line (Warburg impedance) at low-frequency range. The same EC was employed to fit all of the impedance data in 1 M NaOH solution. To improve the fit and minimize the error, the impedance data of ODT-coated zinc electrodes were fitted to  $R[QR(RW)]$  that was proposed by Fawcett<sup>21</sup> to simulate thiol/Au systems in the presence of a redox couple in solution. The fitting and calculation results are listed in Table 3.

As presented in Table 3, the ODT monolayer-modified zinc electrodes displayed higher  $R_{ct}$  values than that of bare zinc electrodes. For instance, the values of  $R_{ct}$  of ODT/Zn<sub>re</sub> electrodes are, respectively, 833, 4028, and 34.2 W in 0.1 M HCl, 0.5 M NaCl, and 1 M NaOH solutions, yielding a corresponding protection efficiencies of 95.4, 90.8, and 84.1%. In the case of ODT/Zn<sub>ox</sub>, the protection efficiencies are 93.4, 99.0, and 70.5% in 0.1 M HCl, 0.5 M NaCl, and 1 M NaOH solutions, respectively. These results indicate that thiol monolayers provide effective corrosion protection to underlying zinc at the early immersion stage in different media. However, we have to note that  $R_{SAM}$  and  $R_{ct}$  reduced quickly with immersion time in solution, indicating the failure of protection probably due to the presence of the defects within the ODT monolayers. For example, in the case of the ODT/Zn<sub>re</sub> electrode immersion in 0.5 M NaCl solution, the EIS measurements (not shown) revealed that  $R_{SAM}$  and  $R_{ct}$  reduced within 1 h from 32 and 4.0 kWcm<sup>-2</sup> to 1.1 and 1.5 kWcm<sup>-2</sup>, respectively.

Assuming that alkanethiol monolayers at the metal surface are defect-free films and ignoring the electron tunneling effect, the films should behave just like a pure capacitor. The Nyquist plot of a defect-free film would appear as a straight line, other than a ( $R_{ct}Q_{dl}$ ) loop, which is perpendicular to (ideal capacitor,  $C$ ) or tilted (constant phase element,  $Q$ ) to the  $Z_{re}$ -axis in a complex plane. However, if the thiol monolayers contains some defects (e.g., pinholes and collapsed sites), corrosive ions in the solution may access the metal substrate through those defects, which can lead to pitting corrosion and to an obvious decrease in charge-transfer resistance. The initial pitting corrosion may expand and spread, resulting in further destruction

of the monolayer<sup>41</sup> and a continuous decrease in charge-transfer resistance. In this work, there is some evidence indicating the presence of pinholes and/or collapsed sites within the ODT monolayer, despite the coverage of ODT at the Zn surface ( $5.4 \times 10^{14}$  molecules/cm<sup>2</sup>), which is slightly higher than that of at the Au surface ( $7.6 \times 10^{-10}$  mol/cm<sup>2</sup> =  $4.6 \times 10^{14}$  molecules/cm<sup>2</sup>).<sup>42</sup> First, (*RQ*) loops instead of straight lines were observed in the Nyquist plots for all of the ODT-modified zinc electrodes (see Figure 6). Second, the values of  $R_{ct}$  for ODT-modified Zn electrodes decreased with the immersion time and the increase of the corrosive nature of electrolyte. These results indicate the presence of defects within ODT monolayers. When aggressive ions reach the Zn substrate through those defects, protection fails and corrosion takes place. Moreover, the observation of methylene group resonances in SFG spectra (see Figure 2) also demonstrates the presence of defects within ODT monolayers at the zinc electrodes.

### Conclusion

ODT was modified to electrochemically reduce Zn and thermally and electrochemically oxidized Zn surfaces. On the basis of SFG and EIS measurements, ODT could adsorb at either reduced Zn or oxidized Zn surfaces to form ordered monolayers. In ppp-SFG spectra, three strong methyl group resonances and two weak methylene group resonances appearing as peaks were observed. After modification of the ODT monolayers, the interfacial capacitances decreased dramatically and the charge-transfer resistances increased significantly for the zinc electrodes. All of the evidence obtained in this work demonstrates the formation of the ordered ODT monolayers at the Zn surfaces. A 0° cant angle for the alkane chain of ODT at the Zn surface was deduced from EIS measurements. Moreover, CV and SFG investigations revealed that the ODT monolayer at the Zn surface undergoes reductive desorption at -1.66 V in 0.5 M NaOH and at -1.62 V in 0.5 M NaClO<sub>4</sub> solutions. The charge consumed to desorption ODT from the Zn electrode was determined as 87 mC/cm<sup>2</sup> from the CV curve that corresponds to a coverage of  $9.0 \times 10^{-10}$  mol/cm<sup>2</sup> ( $5.4 \times 10^{14}$  molecules/cm<sup>2</sup>) if assuming that the reduction follows a one-electron process. There is no obvious CV and SFG evidence showing that reductive desorption of the ODT monolayer takes place in 0.5 M HClO<sub>4</sub> solution. Finally, EIS data analysis indicated that the ODT monolayers at the Zn surface effectively inhibit the corrosion of the zinc in base, salt, and acid media at the early immersion stage. However, the protection efficiency reduced with immersion time due to the presence of the defects within the monolayers.

**Acknowledgment.** This work is supported by Champion Technologies (Houston) and Texas Advanced Technology Program (ATP) under Grant No. 003652-0044.

### References and Notes

- Mekhalif, Z.; Massi, L.; Guittard, F.; Geribaldi, S.; J., D. *Thin Solid Films* **2002**, *405*, 186.
- Love, J. C.; Estroff, L. A.; Kriebel, J. K.; Nuzzo, R. G.; Whitesides, G. M. *Chem. Rev.* **2005**, *105*, 1103.
- Volmer-Uebing, M.; Stratmann, M. *Appl. Surf. Sci.* **1992**, *55*, 19.
- Ruan, C. M.; Bayer, T.; Meth, S.; Sukenik, C. N. *Thin Solid Films* **2002**, *419*, 95.
- Zhang, H. P.; Romero, C.; Baldelli, S. *J. Phys. Chem. B* **2005**, *109*, 15520.
- Mekhalif, Z.; Riga, J.; Pireaux, J.-J.; Delhalle, J. *Langmuir* **1997**, *8*, 22285.
- Keller, H.; Simak, P.; Schrepp, W.; Dembowski, J. *Thin Solid Films* **1994**, *244*, 799.
- Ron, H.; Rubinstein, I. *Langmuir* **1994**, *10*, 4566.
- Ron, H.; Cohen, H.; Matlis, S.; Rappaport, M.; Rubinstein, I. *J. Phys. Chem. B* **1998**, *102*, 9861.
- Himmelhaus, M.; Gauss, I.; Buck, M.; Eisert, F.; Woll, C.; Grunze, M. *J. Electron Spectrosc. Relat. Phenom.* **1998**, *92*, 139.
- Li, Z. Y.; Chang, S.-C.; Williams, R. S. *Langmuir* **2003**, *19*, 6744.
- Karsi, N.; Lang, P.; Chehimi, M.; Delamar, M.; Horowitz, G. *Langmuir* **2006**, *22*, 3118.
- Cabot, P. L.; Cortes, M.; Centellas, F. A.; Garrido, J. A.; E., P. *J. Electroanal. Chem.* **1986**, *201*, 85.
- Goff, A. H.; Joiret, S.; Saidani, B.; Wiart, R. *J. Electroanal. Chem.* **1989**, *263*, 127.
- Zhang, X. G. *Corrosion and Electrochemistry of Zinc*; Plenum Press: New York and London, 1996.
- Cai, W.-B.; Scherson, D. A. *J. Electrochem. Soc.* **2003**, *150*, B217.
- Shan, X.; Ren, D.; Scholl, P.; Prentice, G. *J. Electrochem. Soc.* **1989**, *136*, 3594.
- Bain, C. D. *J. Chem. Soc., Faraday Trans* **1995**, *91*, 1281.
- Ward, R. N.; Duffy, D. C.; Davies, P. B.; Bain, C. D. *J. Phys. Chem.* **1994**, *98*, 8536.
- Hines, M. A.; Todd, J. A.; Guyot-Sionnest, P. *Langmuir* **1995**, *11*, 493.
- Protsailo, L. V.; Fawcett, W. R. *Electrochim. Acta* **2000**, *45*, 3497.
- Janek, R. P.; Fawcett, W. R.; Ulman, A. *J. Phys. Chem. B* **1997**, *101*, 8550.
- Diao, P.; Guo, M.; Rong, R. T. *J. Electroanal. Chem.* **2001**, *495*, 98.
- Slowinski, K.; Chamberlain, R. V.; Miller, C. J.; Majda, M. *J. Am. Chem. Soc.* **1997**, *119*, 11910.
- Hsu, C. H.; Mansfeld, F. *Corrosion* **2001**, *57*, 747.
- Walczak, M. M.; Popenoe, D. D.; Deinhammer, R. S.; Lamp, B. D.; Chung, C.; Porter, M. D. *Langmuir* **1991**, *7*, 2687.
- Schneider, T. W.; Buttry, D. A. *J. Am. Chem. Soc.* **1993**, *115*, 12391.
- Imabyashi, S.-I.; Hobar, D.; Kakiuchi, T.; Knoll, W. *Langmuir* **1997**, *13*, 4502.
- Zhong, C.-J.; Porter, M. D. *J. Electroanal. Chem.* **1997**, *425*, 147.
- Yang, D.-F.; Wilde, C. P.; Morin, M. *Langmuir* **1997**, *13*, 243.
- Yang, D.-F.; Morin, M. *J. Electroanal. Chem.* **1998**, *441*, 173.
- Kawaguchi, T.; Ysuda, H.; Shimazu, K.; Porter, M. D. *Langmuir* **2000**, *16*, 9830.
- Mulder, W. H.; Calvente, J. J.; Andreu, R. *Langmuir* **2001**, *17*, 3273.
- Munakata, H.; Oyamatsu, D.; Kuwabata, S. *Langmuir* **2004**, *20*, 10123.
- Shepherd, J. L.; Kell, A.; Chung, E.; Sinclair, C. W.; Workentin, M. S.; Bizzotto, D. *J. Am. Chem. Soc.* **2004**, *126*, 8329.
- Caswell, P.; Hampson, N. A.; Larkin, D. *J. Electroanal. Chem.* **1969**, *20*, 335.
- Laibinis, P. E.; Whitesides, G. M. *J. Am. Chem. Soc.* **1992**, *114*, 9022.
- Feng, Y.; Teo, W.-K.; Siow, K.-S.; Gao, Z.; Tan, K.-L.; Hsieh, A.-K. *J. Electrochem. Soc.* **1997**, *144*, 55.
- Ma, H. Y.; Yang, C.; Chen, S. H.; Jiao, Y. L.; Huang, S. X.; Li, D. G.; Luo, J. L. *Electrochim. Acta* **2003**, *48*, 4277.
- Grundmeier, G.; Reinartz, C.; Rohwerder, M.; Stratmann, M. *Electrochim. Acta* **1998**, *43*, 165.
- Zamborini, F. P.; Crooks, R. M. *Langmuir* **1998**, *14*, 3279.
- Widrig, C. A.; Alves, C. A.; Porter, M. D. *J. Am. Chem. Soc.* **1991**, *113*, 2805.